03,07,08

Surface morphology and growth processes of germanium films synthesized by solid-phase epitaxy on $Fe_3Si|Si(111)$

© A.V. Lukyanenko, A.V. Tsarenko, I.A. Yakovlev, A.S. Tarasov

Kirensky Institute of Physics, Federal Research Center KSC SB RAS,
Krasnoyarsk, Russia

E-mail: lav@iph.krasn.ru

Received October 23, 2025
Revised November 15, 2025
Accepted December 15, 2025

This work investigates the structural properties of ferromagnet/semiconductor multilayer films synthesized on silicon substrates, specifically examining the growth processes of germanium films on Fe_3Si during solid-phase epitaxy. It has been established that annealing of a nanocrystalline germanium layer with a thickness of less than 25 nm at a temperature of 370 °C leads to the formation of monocrystalline islands with identical crystallographic orientation. The influence of annealing time, germanium layer thickness, and combined synthesis methods on the crystallization processes has been determined. In the stationary regime, the surface diffusion length of germanium adatoms is approximately 1800 nm.

Keywords: hybrid structures, thin films, molecular beam epitaxy, solid-phase epitaxy, high-energy electron diffraction, atomic force microscopy.

DOI: 10.61011/PSS.2026.01.63234.294-25

1. Introduction

The development of spintronics, based on controlling the spin of an electron rather than its charge, opens up prospects for creating a new generation of electronic devices characterized by increased performance and reduced energy consumption [1]. The key components of such devices are magnetic tunnel junctions and spin valves [2,3], created on the basis of structures ferromagnet/metal/ferromagnet and ferromagnet|semiconductor|ferromagnet (FM|SC|FM) [4,5]. Vertical structures of FM|SC|FM are particularly attractive due to their compactness and the possibility of a high degree of integration into semiconductor electronics [6,7]. Ferromagnetic layers are a source of spin-polarized electrons and make it possible to create elements of magnetoresistive random access memory (MRAM) [8], magnetic field sensors [9] and neuromorphic systems [10] that simulate the work of the brain.

Among ferromagnetic materials, Heusler compounds are of particular interest, having a unique combination of magnetic and electronic properties [11–13]. The efficiency of devices based on FM|SC|FM heterostructures largely depends on the atomic perfection of the interfaces and the crystalline quality of layers [14]. The use of ferromagnetic silicide Fe_3Si with a crystal structure of $D0_3$ and a lattice parameter close to the size of basic semiconductors [15], allows the creation of high-quality epitaxial heterostructures on substrates GaAs [4,16], Ge [17] and Si [18–21].

The combination of ferromagnetic Heusler compounds with semiconductors, in particular, with germanium is of practical interest since it has a higher mobility of charge carriers than silicon and is compatible with modern silicon technology [22,23]. However, the key problem remains controlled epitaxial germanium growth on ferromagnetic materials, where surface diffusion and nucleation processes play a crucial role. The selection of materials potentially allows creating better interfaces: the silicide Fe_3Si has an exceptionally small ($\sim 0.08\,\%$) mismatch of the lattice parameters with Ge. However, the epitaxial growth of a semiconductor on a metal surface Fe_3Si is fraught with serious technological difficulties. The main difficulty lies in the incompatibility of the thermodynamic growth conditions: to obtain crystalline Ge, relatively high temperatures are required, at which the metal surface is prone to dissociation, chemical reactions, and mutual diffusion [16]. This leads to the formation of rough interfaces and impurities, which reduces the efficiency of spin transport through the barrier.

Several approaches to obtaining monocrystalline germanium on silicide are described in the literature. The epitaxial growth of Ge films was controlled in Ref. [24] by the upper layer of silicide atoms. At the Si-terminations of the Fe_3Si layers, it is possible to obtain sufficiently smooth Ge films (with RMS roughness $R_{RMS} \approx 0.41$ nm), whereas three-dimensional epitaxial growth of Ge films was observed on the surface of Fe_3Si with the Fe-termination. The structural properties of the Ge film and the upper layer Fe_3Si depend on the substrate temperature during deposition of Ge [4]. The low-temperature growth of Ge ($\sim 150\,^\circ$C) makes it possible to keep the interface between Ge and Fe_3Si films clear, without atom diffusion (the so-called sharp interface), but germanium films remain amorphous, whereas the temperature of $\sim 325\,^\circ$C ensures the epitaxial growth, but is accompanied by an increase in roughness and disorientation of crystallites. A promising method is the

Table 1. Technological parameters

Name of sample	Thickness Ge, nm	Temperature of sputtering, °C	Temperature of annealing, °C	Time of annealing, min
S0Ge5RT	5	RT	–	–
S0Ge5	5	370	–	–
S0Ge10	10	370	–	–
S1t90	5	RT	370	90
S1t280	5	RT	370	280
S1t280*	5	RT	360	280
S2Ge7	7	RT	370	280
S2Ge10	10	RT	370	670
S2Ge20	20	RT	370	930
S3Ge7++	7+7+7	RT	370	360+210+
S3Ge5+	5+	370	370	680
S3Ge10+	10+	370	370	670

reduction of the germanium growth temperature by doping with tin (Sn) [20].

The hybrid method combining deposition of amorphous Ge onto a cooled Fe_3Si substrate followed by controlled annealing makes it possible to minimize interfacial diffusion and form sharp atomically smooth interfaces. The introduction of a Ge layer grown by solid-phase epitaxy (SPE) [21] ensures two-dimensional epitaxial growth at a temperature of $\sim 175\,^{\circ}$C. Slow annealing at temperatures from 240 to 380 °C makes it possible to obtain germanium films with $R_{RMS} \approx 1$ nm [16].

Despite significant progress, there are still unresolved issues related to the influence of various annealing modes on the crystallization process of Ge. There are no systematic studies of the surface diffusion of Ge atoms on single crystal surfaces of Fe_3Si using direct observation methods such as scanning tunneling microscopy or atomic force microscopy (AFM). The main focus is on volumetric diffusion and processes at interfaces in complex heterostructures. Existing work on germanium surface diffusion is usually limited to studies on silicon substrates at high temperatures [25,26].

This paper presents the results of studying the crystallization processes of germanium films on $Fe_3Si|Si(111)$ at an annealing temperature of 370 °C. The influence of various technological parameters has been studied using the methods of *in-situ* reflection high-energy electron diffraction (RHEED) and *ex-situ* AFM. The experimental RHEED patterns are compared with the calculated electron diffraction patterns for a single crystal of Ge. Conclusions about the kinetics of crystallization processes were drawn from the analysis of AFM images, which allowed obtaining new information about the mechanisms of germanium crystallization on the surface of iron silicide.

2. Methods

The samples were synthesized under ultrahigh vacuum conditions (base vacuum $1.3 \cdot 10^{-7}$ Pa) by molecular beam epitaxy (MBE) followed by annealing. The evaporation of materials (iron, silicon, germanium) was carried out from thermal sources such as „Knudsen effusion cells“ with crucibles of boron nitride. At the first stage, a layer of Fe_3Si silicide with a thickness of 10 nm was sputtered onto the cleaned Si(111) substrate 7×7 at a temperature of 150 °C the co-deposition of iron and silicon according to a proven method [27], after that the sample was cooled to room temperature for 180 min. At the next stage, a layer of germanium of a given thickness was sputtered at room temperature (RT) and a flow rate of 0.033 Å/s, after which a smooth heating was carried out to a temperature of 370 °C at a rate of 10 K/min. The technological thickness of the germanium layer and the annealing mode for each sample are shown in Table 1.

The change in the crystal structure during synthesis was continuously monitored by *in situ* RHEED method. After synthesis, the samples were cooled to room temperature in two stages to minimize further surface processes: rapid temperature decrease from 370 to 150 °C at a rate of 10 K/min and slow cooling to RT for 120 min at a rate of 1 K/min. After that, the samples were evacuated from the vacuum chamber, and the surface morphology was *ex situ* studied using AFM in semi-contact scanning mode by DPN 5000 (NanoInk) system. NSG10 (Tips Nano) cantilevers were used for the studies. Image processing and statistical values were obtained using the free software Gwyddion 2.65 [28] and ImageJ [29]. The main statistical parameters obtained from AFM data are listed in Table 2.

Table 2. Statistical values

Name of sample	Thickness Ge (izACM), nm	Average height of crystals Ge $\langle h \rangle$, nm	Average diameter $\langle d \rangle$, nm	Coating of surface, %
S0Ge5RT	–	–	–	–
S0Ge5	–	14.7 ± 1.7	471.6	26.6
S0Ge10	–	17.6 ± 2.6	811.4	39.1
S1t90	2.7 ± 0.3	11.1 ± 1.8	391.6	3.9
S1t280	2.5 ± 0.4	12.7 ± 1.0	594.2	19.4
S1t280*	2.6 ± 0.3	15.2 ± 1.7	603.2	6.9
S2Ge7	4.2 ± 0.6	15.1 ± 2.4	1643.0	32.1
S2Ge10	7.8 ± 0.5	19.3 ± 1.9	–	10.0
S2Ge20	16.1 ± 0.7	29.2 ± 3.3	1086.4	51.5
S3Ge7++	15.1 ± 1.0	27.7 ± 2.3	1621.3	34.7
S3Ge5+	–	28.3 ± 8.0 51.5 ± 6.0	1180.1 326.9	12.5 21.6
S3Ge10+	–	45	15	–

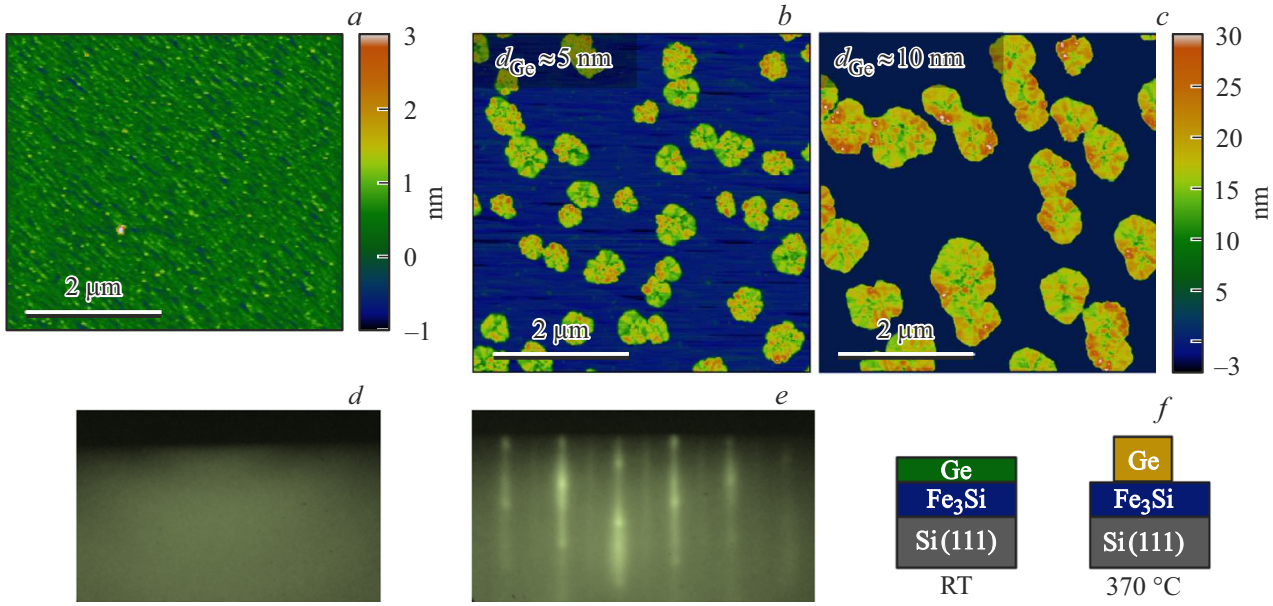

Figure 1. AFM images of the surface of Ge films grown on the surface of $Fe_3Si(111)$ obtained under various technological conditions. *a*) S0Ge5RT sample, deposition of Ge on the surface of Fe_3Si at room temperature; *b*) $S0Ge_5$ sample, deposition of 5 nm of Ge at a temperature of 370 °C; *c*) S0Ge10 sample, deposition of 10 nm of Ge at a temperature of 370 °C. The range of the pseudo-color scale for (*b*) and (*c*) is set to be the same and ranges from −3 to 30 nm. RHEED patterns from samples: *d*) S0Ge5RT, *e*) S0Ge5. *f*) A diagram of the layers obtained as a result of experiments.

3. Results

At the first stage, the crystal structure and morphology of the germanium film surface were compared after deposition on Fe_3Si under various temperature conditions. The experimental samples is shown in Figure 1, *f*. Figure 1, *a*–*c* shows AFM images for three different samples: S0Ge5RT sample with a 5 m thick Ge layer deposited at RT (Figure 1, *a*); S0Ge5 and S0Ge10 samples with germanium layer thicknesses of 5 and 10 nm, respectively, grown at a substrate temperature of 370 °C (Figure 1, *b* and *c*). Figure 1, *d*, and *e* show RHEED patterns for S0Ge5RT and S0Ge5

samples, which correlate with AFM microscopy data and allow evaluating the crystallinity of the synthesized films. The diffraction pattern (Figure 1, *d*) shows only diffuse Debye rings of low intensity, which indicate the formation of a nanocrystalline structure in a film where the grain size does not exceed several nanometers. According to the AFM data for S0Ge5RT, the formation of a continuous uniform germanium layer is observed, the surface morphology of which is determined by the underlying layer of iron silicide, the value of $R_{\mathrm{RMS}} \approx 0.19$ nm.

The diffraction pattern from the S0Ge5 sample with a technological thickness of 5 nm germanium deposited at a temperature of 370 °C (Figure 1, *e*) shows the appearance of point reflections against the background of a picture from a single-crystal film Fe_3Si. This indicates the formation of monocrystalline islands of the same orientation on the surface of the silicide. With an increase in the technological thickness of germanium to 10 nm (sample S0Ge10), no changes are observed in the RHEED pattern compared to S0Ge5. To identify the point reflexes, an electron diffraction pattern was calculated for a germanium single crystal (Fdm type lattice with parameter $a = 0.556$ nm) in the direction of the zone axis $\langle 110 \rangle_{\mathrm{Ge}}$ (Figure 2, *d*), the reflexes of which completely coincide with point reflexes in the RHEED pattern. A two-dimensional AFM image of Ge crystals of the same height for S0Ge5 sample can be observed on Figure 1, *b*. When 5 nm germanium is deposited on Fe_3Si at a temperature of 370 °C, randomly arranged flat germanium crystals with a height of ~ 15 nm are formed, the average distance between which is ~ 470 nm. The crystals cover 26.6 % of the surface, and their average size is ~ 471.6 nm. This shape of the islands indicates that growth in the lateral direction occurs faster than in the direction normal to the substrate plane, which leads to the formation of flat crystals. Figure 1, *c* shows an image for sample S0Ge10 when twice as much germanium (10 nm) was deposited at a temperature of 370 °C. There is a clear dependence of the lateral size of the germanium islands on the technological thickness of Ge. The crystals are on average ~ 18 nm in height, and the average crystal size is ~ 811 nm. Due to coalescence, the average distance between the crystals increases and amounts to ~ 520 nm, while they occupy ~ 39.1 % of the surface. AFM exhibits points on the surface of the silicide are noticeable (usually located on ridges); perhaps these are nucleation centers that formed during the cooling of the substrate.

Since the formation of separately arranged monocrystalline flat Ge islands is observed during the annealing process, several series of samples were obtained for a more detailed study of the Ge crystallization process to study various factors affecting the germanium film growth process. In the first series, the effect of annealing time on the crystal structure and morphology of the surface was studied; in the second, the effect of the thickness of the germanium nanocrystalline layer was studied; in the third, the growth processes realized with combined synthesis methods were studied: the sequential SPE process and germanium deposition on a preheated substrate containing formed germanium crystals. Table 1 shows the main technological characteristics of the obtained samples.

3.1. Effect of annealing time

After deposition of the germanium layer at room temperature, the samples S1t90 and S1t280 were annealed at a temperature of 370 °C for 90 and 280 min, respectively. The technological thickness of the nanocrystalline germanium layer is 5 nm. When studying the crystal structure of the film by RHEED during annealing, the following was found: 60 min after the start of heating, elongated reflexes began to appear on the diffraction pattern (not presented in the article)-„streaks“ of weak intensity against the background of diffuse Debye rings from a germanium nanocrystalline film; after 90 min (sample S1t90) of heating and annealing two groups of reflexes are observed on the diffraction pattern („streaks“ and dots) (Figure 2, *a*); no visible changes are observed in the RHEED pattern with further annealing to 280 min (sample S1t280). Analysis of the diffraction data suggests that the group of elongated reflections„„streaks“ belongs to the single-crystal surface of the silicide Fe_3Si [27] with a slight roughness. The group of point reflexes is described by the monocrystalline structure of germanium (Figure 2, *d*). The transformation of the diffraction pattern during annealing from diffuse rings to reflexes of two different types, which correspond to the smooth surface of the silicide Fe_3Si and monocrystalline islands of Ge, may indicate that the germanium layer at the annealing temperature 370 °C begins to crystallize into islands, revealing the surface of the underlying layer silicide. For all subsequent samples, the RHEED patterns during annealing visually had the same geometry as in Figure 2, *a*, so they are also not presented in the article, the difference was only in the different time of the onset of reflexes during annealing.

Figure 2, *b* shows that annealing at 370 °C initiates the crystallization process (sample S1t90). The formation of germanium crystals with a size of ~ 391.6 nm is observed after annealing for 90 min, including the heating time, while the crystals occupy a small part of the surface, and 92.5 % is covered with a layer of nanocrystalline germanium with a thickness of ~ 2.5 nm. Figure 2, *e* shows typical cross-sectional profiles of AFM images for samples S1t90 and S1t280. The region around the crystals free from the Ge layer correlates with the length of the surface diffusion of Ge adatoms. The formation of secondary crystallization centers and the gradual growth of new crystals are observed, the linear sizes of germanium crystals increase (S1t280, Figure 2, *c*) with a long annealing time of $t_{\mathrm{annealing}} \approx 280$ min. Two typical distances between crystals can be distinguished (~ 500 and ~ 1500 nm), in the Table 2 shows the average value. The germanium layer still covers 10% of the surface of the silicide.

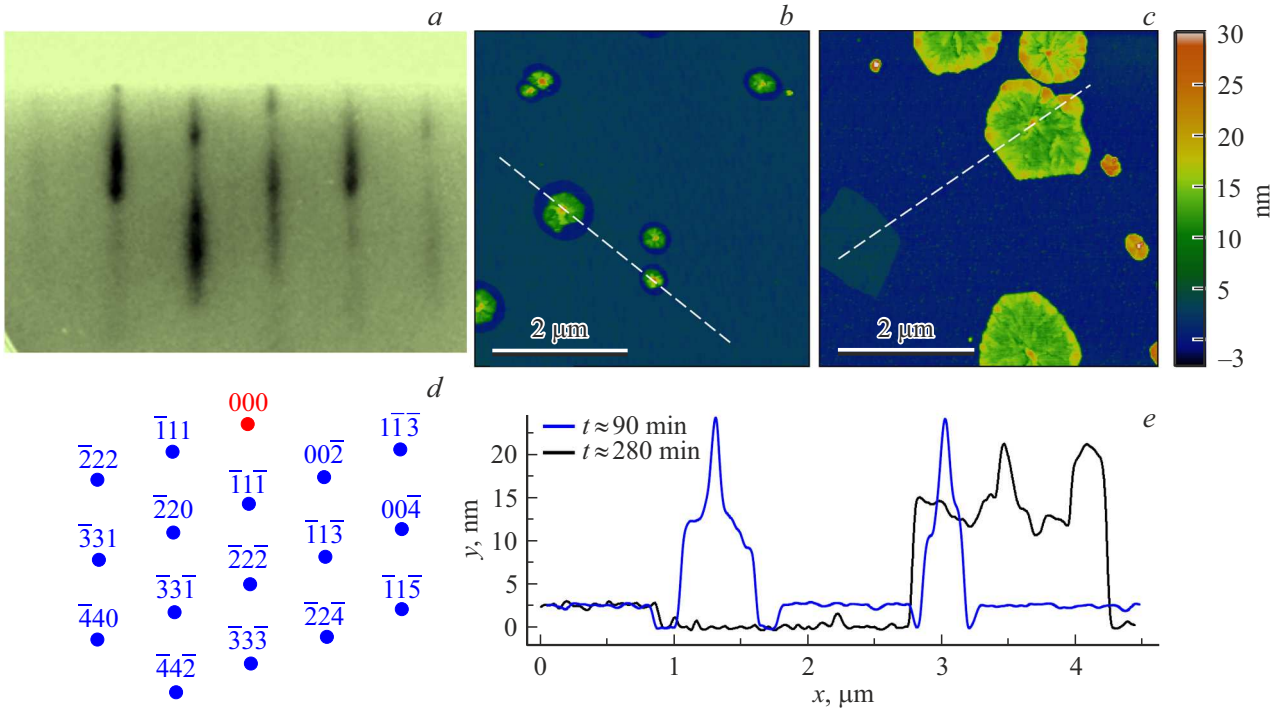

Figure 2. RHEED pattern and AFM images for samples S1t90 and S1t280. *a*) Experimental RHEED pattern from Ge|Fe_3Si|Si(111) after annealing at a temperature of 370 °C for 90 min; *b*) AFM image of sample S1t90, after annealing for 90 min; *c*) AFM image of sample S1t280, after annealing for 280 min. The dotted line marks the extracted profiles. *d*) Calculated electron diffraction pattern for a Ge single crystal in the direction of the band axis ⟨110⟩Ge. *e*) Cross-section profiles for samples S1t90 and S1t280.

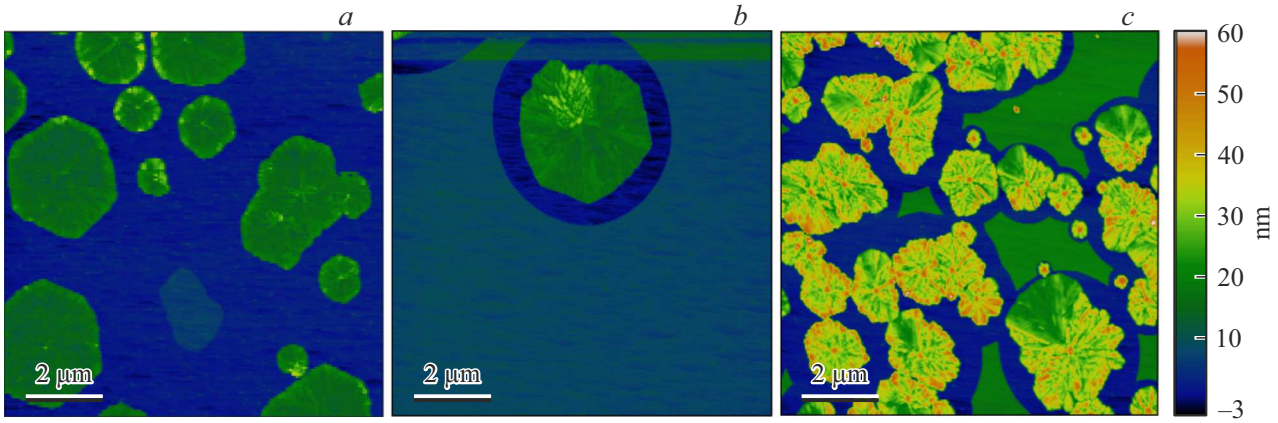

Figure 3. Germanium crystals on the surface of Fe_3Si depending on the thickness of the nanocrystalline Ge. The technological layer thickness is 7, 10 and 20 nm for samples *a*) S2Ge7, *b*) S2Ge10 and *c*) S2Ge20. The range of the pseudo-color range is from −3 to 60 nm.

3.2. Effect of nanocrystalline germanium layer thickness

According to RHEED data, the annealing time required to initiate crystallization of the germanium layer demonstrates a strong dependence on the layer thickness, increasing by an order of magnitude from 60 to 600 min with an increase in thickness from 5 to 20 nm. According to the AFM data (Figure3), the larger the germanium layer, the larger the crystals after annealing. An increase in the thickness of germanium (sample S2Ge7, Figure 3, *a*) leads to an increase in the linear crystal sizes to ∼ 1643 nm. Crystals occupy ∼ 32 % of the surface, and a layer of nanocrystalline germanium occupies no more than 3.5 % of the surface. Obtaining a thin solid monocrystalline film by increasing the thickness of the germanium layer is impossible due to the three-dimensional nature of crystallization. Despite the anisotropy of the growth rate (with predominance of growth in the substrate plane), the annealing process leads to the formation of an island film. An increase in the thickness of

the germanium layer to 20 nm (Figure 3, S2Ge20) leads to crystal coalescence during the SPE process. More than 51 % of the surface is covered with crystals, and after 930 min of annealing, 16 % of nanocrystalline germanium remains.

3.3. The effect of additional portions of germanium

The deposition of an additional layer of germanium onto the already formed Ge islands on $Fe_3Si|Si(111)$ was carried out at room temperature followed by annealing (Figure 4, *a* and *d*) and at a temperature of 370 °C (Figure 4, *b* and *c*). Let's consider each of the cases in detail. The sequential SPE process of new germanium layers on silicide leads to the sequential growth of already formed crystals. Figure 4, *a*, and *d* (sample S3Ge7++) show AFM images of concentric germanium crystals that continue to increase with each subsequent annealing. The images 10×10 and $30\times30\,\mu$m are presented for the S3Ge7++ sample. The corresponding cross-section profiles (Figure 4, *e*) show layers of germanium ~ 15 nm and crystals ~ 27 nm. The deposition of a new portion of germanium during the annealing procedure leads to the appearance of new crystallization centers and subsequent vertical growth. When the length of the surface diffusion is less than the distance between the existing germanium crystals, new growth centers are randomly generated. Figure 4, *b* (S3Ge5+) shows an AFM image which contains crystals of two lateral sizes: large, ~ 1180.1 nm, crystals formed as a result of SPE, and ~ 326.9 nm crystals, obtained by subsequent deposition at ultra-low flow rates of ~ 0.05 nm/min. The twinning of reflexes from Ge begins to manifest itself in the RHEED pattern. In the case of the presence of a layer of nanocrystalline germanium on the surface of the silicide during the deposition of a new portion (Figure 4, *c*, sample S3Ge10+), it seems that the surface diffusion length of Ge adatoms coming from the source is too small and secondary crystallization is initiated more evenly, which leads to form a multitude of small crystals with a size of ~ 15 nm and a height of ~ 45 nm. If the Ge islands begin to approach each other, they impose geometric constraints on the lateral growth of each island [30].

When Ge is deposited on a substrate, the length of the surface diffusion of adatoms affects the size, density, and distribution of the islands formed. A shorter diffusion length leads to a greater number of small islands (high density, low diffusion coefficient). A longer diffusion length leads to fewer large islands (low density, high diffusion coefficient). During thermal annealing, Ge adatoms diffuse over the surface from the germanium layer to a randomly generated island, which leads to anisotropic radial growth. The thickness of the Ge islands varies much more slowly.

Despite minor changes in technological parameters (Table 1) and identical RHEED patterns (Figure 2, *a* and *d*), morphology of germanium crystals (Table 2) is quite diverse. This observation highlights the limitations of exclusively diffraction methods for the complete characterization of thin films. Previously in the literature in the formation of multilayer heterostructures of FM/SC for the germanium layer, only RHEED data were described, and only in rare cases the values of R_{RMS} of the upper layer were given. Additional AFM data may be useful for a better understanding of the ongoing processes. In turn, the quality of the subsequent ferromagnetic Fe_3Si layer depends on the morphology and crystalline state of the germanium layer surface, which determines the final functional characteristics of the entire heterostructure.

4. Discussion

The main kinetic parameters (activation energy E_s, surface diffusion coefficient D_s) were determined taking into account the assumptions that the island densities Ge at the saturation stage does not depend on the gradient of the chemical potential. Therefore, the surface diffusion of adatoms is the dominant factor determining the island density. An analytical model was proposed in Ref. [25] that relates the average island size to kinetic parameters, and a method was proposed for determining the surface diffusion coefficient and activation energy of Ge adatoms.

Additionally, a sample S1t280* was obtained, identical to S1t280, but at a lower annealing temperature of 360 °C. The concentration of islets (N_{island}) was determined by counting all islets (regardless of stage) on the AFM frames shown in Figures 5, *a* and *b*. This parameter shows how many islands there are per unit area. For a temperature of 360 and 370 °C N_{island} it is $N^{360}_{\mathrm{island}} \approx 1.08\cdot10^7\,\mathrm{cm}^{-2}$ and $N^{370}_{\mathrm{island}} \approx 3.24\cdot10^7\,\mathrm{cm}^{-2}$,respectively. It is possible that the values obtained are underestimated due to the processes of nucleation, which lead to the merging and enlargement of the islands. In addition, the resolution of the AFM method is limited, and when scanning large areas, islands smaller than the critical size could be missed, which could also affect the calculations.

The surface flux of Ge (J) adatoms was estimated based on the analysis of AFM images for samples S1t90 and S1t280 with different annealing times (Figure 2, *b* and *c*). During the annealing time ($\Delta t = 190\,\mathrm{min} = 11400\,\mathrm{s}$), the average volume of the island $\langle v\rangle = (\pi d^2)/4\langle h\rangle$ increases from $1.4\cdot10^6\,\mathrm{nm}^3$ ($\sim 63\cdot10^6$ atoms) to $3.5\cdot10^6\,\mathrm{nm}^3$ ($\sim 155\cdot10^6$ atoms). During calculations, it was assumed that the islands have the shape of flat cylinders, however, as can be seen from the AFM data and cross-section profiles (Figure 2, *e* and 4, *e*), the Ge islands have the shape of irregular hexagons and a pronounced peak in the center. Provided that the volume of one atom is Ge $\approx 0.0226\,\mathrm{nm}^3$, the average growth rate of the island is $\Delta n/\Delta t \approx 8070$ atom/s. The following considerations were used to calculate J, i.e. the number of (n) atoms per unit area per unit time. Since the island density is known at 370 °C ($N^{370}_{\mathrm{island}}$) and assuming that each island grows at the rate of $\Delta n/\Delta t$, then $J = (\Delta n/\Delta t)N_{\mathrm{island}} \approx 0.0026$ atoms/$(\mathrm{nm}^2\cdot\mathrm{s}) = 2.6\cdot10^{11}$ atoms/$(\mathrm{cm}^2\cdot\mathrm{s})$. The value of the flow velocity is quite small, since in our

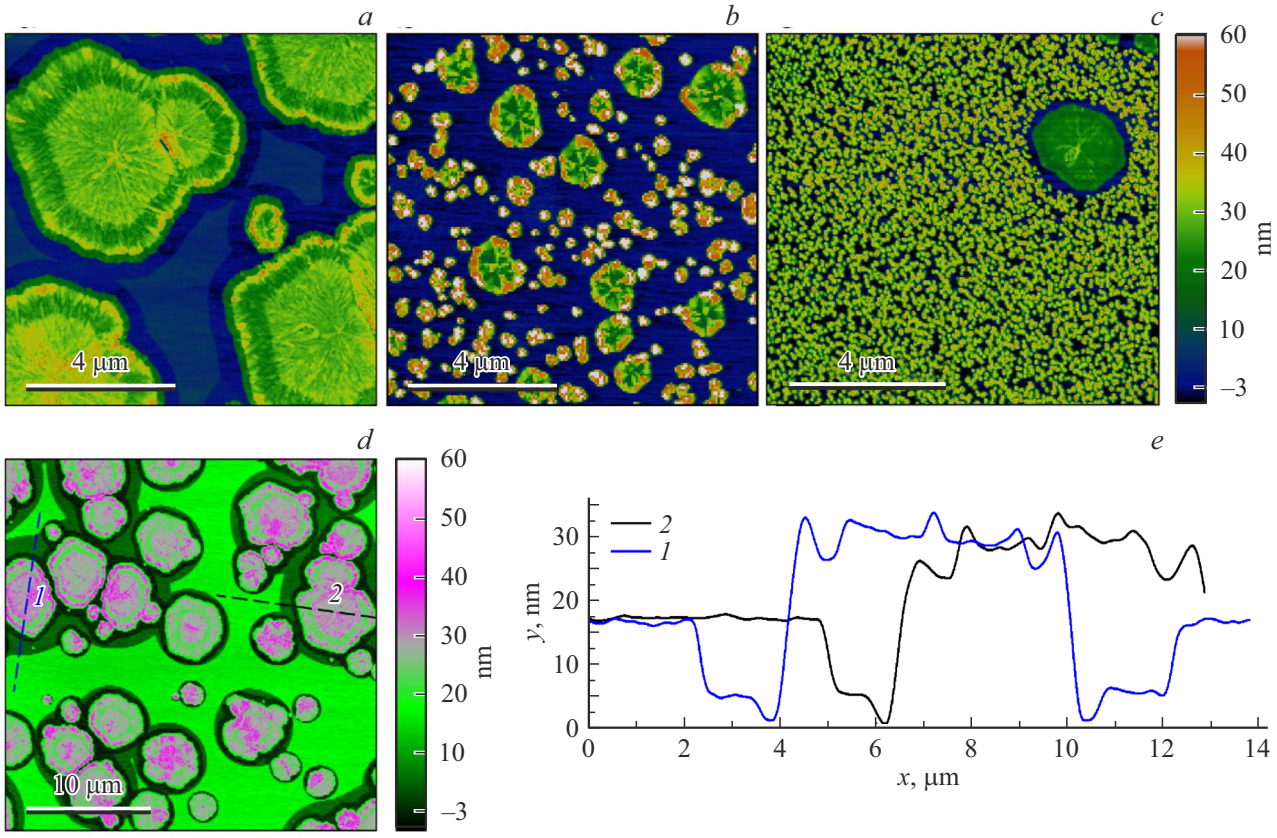

Figure 4. AFM images for samples obtained by combining the processes of MBE growth and SPE. *a, d, e*) S3Ge7++ — three-fold repetition of the deposition procedure at RT and annealing at 370 °C. *b*) S3Ge5+ and *c*) S3Ge10+ — deposition of a new portion of germanium during the annealing procedure in the absence and presence of a germanium layer, respectively. The range of the pseudo-color range is from −3 to 60 nm.

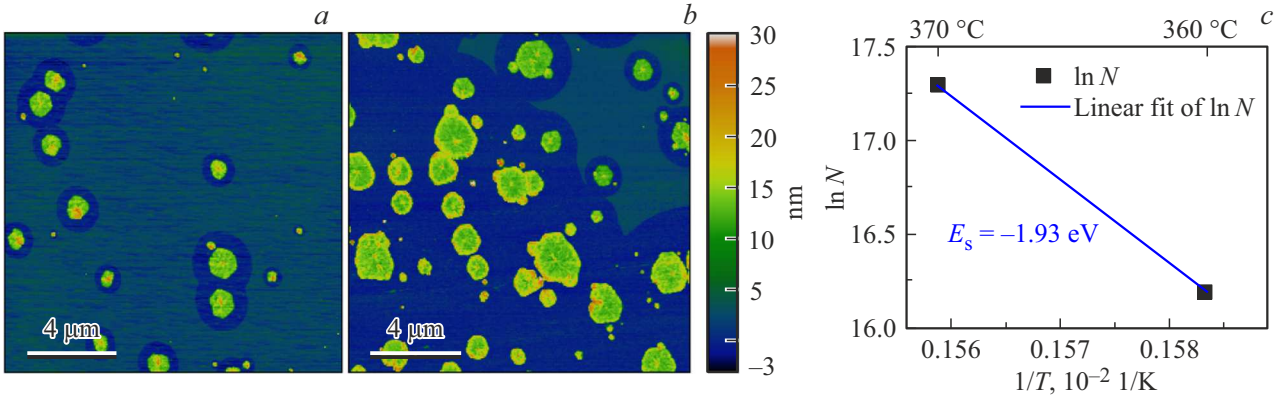

Figure 5. *a* and *b*) Representative AFM frames of $15 \times 15\,\mu m^2$ for samples S1t280* and S1t280. The pseudo-color scale ranges from −3 to 30 nm. *c*) Arrhenius plot (squares) showing the dependence of the density of randomly nascent islands on temperature at the same annealing time $t_a = 280$ min.

case there is only a flow of adatoms from a layer of nanocrystalline germanium. The activation energy value $E_s = -1.93$ eV was obtained using the expression $N_{island} \propto \exp((2E_s)/(k_B T))$, which relates the island density to the activation energy of surface diffusion E_s through the probability of overcoming the energy barrier for nucleation [25]. Figure 5, *c* shows the Arrhenius plot.

The activation energy for surface diffusion is always significantly lower than the activation energy for bulk diffusion, since the energy barriers on the surface are smaller [31]. The negative value of E_s is a consequence of the fact that the concentration of islands increases with increasing temperature, and may indicate a strong bond between Ge and the substrate (Fe_3Si), in contrast to the

classical case [25], when an increase in temperature leads to an increase in the length of surface diffusion and a decrease in the concentration of islands. In classical theory, the density of nucleation centers is inversely proportional to the diffusion length. The higher the substrate temperature, the more energy the adatoms have for diffusion, the further they can migrate. The further the atoms move away from the impact site, the less frequently they occur and form islands.

The surface diffusion coefficient Ds at a temperature of 370 °C can be found using the well-known equation

$$D_s = D_0 \exp(|E_s|/k_B T)$$

$$= D_0 \exp(-1.93/k_B T) = D_0 7.86 \cdot 10^{-16}\,\mathrm{cm}^2/\mathrm{s}$$

(a positive value is inserted into the Arrhenius equation). The main difficulty remains with determining the preexpansion factor D_0, which largely depends on the growth regime. Indirectly, D_s can be estimated from the analysis of AFM data and the formula for the surface diffusion length $\lambda = \sqrt{D_s \tau_s}$, where τ_s is the lifetime of an adatom on the surface. In the stationary mode, when growth is limited by diffusion, $\lambda \sim L$, i.e. the average distance between the islands: $\langle L \rangle = 1824.4 \pm 821.3\,\mathrm{nm} = 1.8 \cdot 10^{-5}\,\mathrm{cm}$ (at 370 °C for samples S1t280 and S1t90). During the time Δt the average path traveled by adatom $\lambda = \sqrt{D_s \Delta t}$, then $D_s \approx \langle L \rangle^2/\Delta t = 2.9 \cdot 10^{-14}\,\mathrm{cm}^2/\mathrm{s}$ and $D_0 = D_s/\exp(|E_s|/k_B T) = 37.1\,\mathrm{cm}^2/\mathrm{s}$. The results obtained are based on a direct relationship between the diffusion length and the average distance between the islands. A more accurate picture can be provided by the diffusion-limited growth model proposed in Ref. [30]. The multiplier D_0 can strongly depend on the growth model and usually the values D_0 for surface diffusion are in the range of $10^{-5}-10^{2}\,\mathrm{cm}^2/\mathrm{s}$ [32]; in our case, the value is within reasonable limits. The coefficient D_s indicates the low mobility of germanium adatoms on the surface of the silicide. Low values of the diffusion coefficient ($10^{-16}-10^{-12}\,\mathrm{cm}^2/\mathrm{s}$) are typical for semiconductors [33].

5. Conclusion

The crystallization processes of continuous nanocrystalline germanium films with a thickness of 5−20 nm on the surface of monocrystalline iron silicide $Fe_3Si|Si(111)$ at a temperature of 370 °C were studied. From the analysis of RHEED and AFM data, it was found that upon heating, the germanium layer crystallizes into single-crystal islands of a flat shape with a crystallographic ratio relative to the substrate $\langle 110 \rangle_{Ge} \parallel \langle 112 \rangle_{Si}$ and $(111)_{Si} \parallel (111)_{Ge}$. It has been experimentally established that the morphology and size of germanium crystals demonstrate a pronounced dependence on the technological parameters of synthesis. As the annealing time increases, the crystal size increases, with a predominance of growth in the lateral direction. As the thickness of the nanocrystalline layer increases, the crystallization start time increases. The use of the combined synthesis method initiates the formation of new crystallization centers, which significantly affects the final microstructure of the film. Based on the quantitative analysis of the AFM data, the kinetic parameters of the SPE process were determined. The surface diffusion coefficient D_s of germanium adatoms on Fe_3Si is $\sim 37.1 \exp(-1.93/k_B T)\,\mathrm{cm}^2/\mathrm{s}$.

Acknowledgments

The authors thank the Krasnoyarsk Regional Research Equipment Sharing Center of the Federal Research Center (FRC) Krasnoyarsk Science Center (KSC) of the Siberian Branch (SB) of the Russian Academy of Sciences (RAS) for the provided equipment.

Funding

The range of research topics under the state assignment of the Kirensky Institute of Physics, SB RAS.

Conflict of interest

The authors declare that they have no conflict of interest

References

[1] I. Žutić, J. Fabian, S.D. Sarma. Rev. Mod. Phys. **76**, *2*, 323 (2004).
[2] S. Bhatti, R. Sbiaa, A. Hirohata, H. Ohno, S. Fukami, S.N. Piramanayagam. Mater. Today **20**, *9*, 530 (2017).
[3] B. Jinnai, K. Watanabe, S. Fukami, H. Ohno. Appl. Phys. Lett. **116**, *16*, 160501 (2020).
[4] B. Jenichen, J. Herfort, U. Jahn, A. Trampert, H. Riechert. Thin Solid Films **556**, 120 (2014).
[5] A.V. Lukyanenko, L.V. Shanidze, M.V. Rautskii, I.A. Yakovlev, A.L. Sukhachev, K.Yu. Maksimova, A.Yu. Goikhman, N.V. Volkov, A.S. Tarasov. Bull. RAS: Phys. **88**, Suppl. *1*, S42 (2024).]
[6] K. Hamaya, Y. Fujita, M. Yamada, M. Kawano, S. Yamada, K. Sawano. J. Phys. D: Appl. Phys. **51**, *39*, 393001 (2018).
[7] A. Yamada, M. Yamada, T. Shiihara, M. Ikawa, S. Yamada, K. Hamaya. J. Appl. Phys. **129**, *1*, 013901 (2021).
[8] S. Ikegawa, F.B. Mancoff, J. Janesky, S. Aggarwal. IEEE Trans. ED **67**, *4*, 1407 (2020).
[9] M.A. Khan, J. Sun, B. Li, A. Przybysz, J. Kosel. Eng. Res. Express **3**, *2*, 022005 (2021).
[10] P. Zhou, A.J. Edwards, F.B. Mancoff, S. Aggarwal, S.K. Heinrich-Barna, J.S. Friedman. Commun. Eng. **4**, *1*, 142 (2025).
[11] G. Hoffmann, J. Herfort, M. Ramsteiner. Phys. Rev. Mater. **3**, *7*, 074402 (2019).
[12] Y.B. Xu, S.S.A. Hassan, P.K.J. Wong, J. Wu, J.S. Claydon, Y.X. Lu, C.D. Damsgaard, J.B. Hansen, C.S. Jacobsen, Y. Zhai, G. van der Laan, R. Feidenhans, S.N. Holmes. IEEE Trans. Magn. **44**, *11*, 2959 (2008).
[13] A.B. Granovskii, V.N. Prudnikov, A.P. Kazakov, A.P. Zhukov, I.S. Dubenko. JETP **115**, *5*, 805 (2012).
[14] T.J. Zega, A.T. Hanbicki, S.C. Erwin, I. Žutić, G. Kioseoglou, C.H. Li, B.T. Jonker, R.M. Stroud. Phys. Rev. Lett. **96**, *19*, 196101 (2006).

[15] W.A. Hines, A.H. Menotti, J.I. Budnick, T.J. Burch, T. Litrenta, V. Niculescu, K. Raj. Phys. Rev. B **13**, *9*, 4060 (1976).
[16] S. Gaucher, B. Jenichen, J. Kalt, U. Jahn, A. Trampert, J. Herfort. Appl. Phys. Lett. **110**, *10*, 102103 (2017).
[17] S. Yamada, K. Tanikawa, M. Miyao, K. Hamaya. Crystal Growth & Design **12**, *10*, 4703 (2012).
[18] A.S. Tarasov, I.A. Tarasov, I.A. Yakovlev, M.V. Rautskii, I.A. Bondarev, A.V. Lukyanenko, M.S. Platunov, M.N. Volochaev, D.D. Efimov, A.Yu. Goikhman, B.A. Belyaev, F.A. Baron, L.V. Shanidze, M. Farle, S.N. Varnakov, S.G. Ovchinnikov, N.V. Volkov. Nanomater. **12**, *1*, 131 (2022).
[19] A.S. Tarasov, A.V. Lukyanenko, I.A. Yakovlev, I.A. Tarasov, I.A. Bondarev, A.L. Sukhachev, L.V. Shanidze, D.A. Smolyakov, S.N. Varnakov, S.G. Ovchinnikov, N.V. Volkov. Bull. RAS: Phys. **87**, Suppl. *1*, S133 (2023).
[20] M. Yamada, S. Kusumoto, A. Yamada, K. Sawano, K. Hamaya. Mater. Sci. Semicond. Process. **171**, 107987 (2024).
[21] S. Sakai, M. Kawano, M. Ikawa, H. Sato, S. Yamada, K. Hamaya. Semicond. Sci. Technol. **32**, *9*, 094005 (2017).
[22] C.J. Palmstrøm. Prog. Cryst. Growth. Charact. Mater. **62**, *2*, 371 (2016).
[23] A.S. Tarasov, I.A. Bondarev, M.V. Rautskii, A.V. Lukyanenko, I.A. Tarasov, S.N. Varnakov, S.G. Ovchinnikov, N.V. Volkov. J. Surf. Investig.: X-ray, Synchrotron & Neutron Techniques **12**, *4*, 633 (2018).
[24] S. Yamada, K. Tanikawa, M. Miyao, K. Hamaya. Crystal Growth & Design **12**, *10*, 4703 (2012).
[25] H.J. Kim, Z.M. Zhao, J. Liu, V. Ozolins, J.Y. Chang, Y.H. Xie. J. Appl. Phys. **95**, *11*, 6065 (2004).
[26] A.E. Dolbak, B.Z. Olshanetsky. Central Eur. J. Phys. **4**, *3*, 310 (2006).
[27] I.A. Yakovlev, S.N. Varnakov, B.A. Belyaev, S.M. Zharkov, M.S. Molokeev, I.A. Tarasov, S.G. Ovchinnikov. JETP Lett. **99**, *9*, 527 (2014).
[28] P. Klapetek, D. Nečas, C. Anderson. Gwyddion user guide. Czech Metrology Institute (2004–2007, 2009).
[29] T.J. Collins. Biotechniques **43**, Suppl. *1*, S25 (2007).
[30] S. Hu, P.C. McIntyre. J. Appl. Phys. **111**, *4*, 044908 (2012).
[31] A.G. Naumovets, Y.S. Vedula. Surf. Sci. Rep. **4**, *7–8*, 365 (1985).
[32] G. Antczak, G. Ehrlich. Surface Diffusion: Metals, Metal Atoms, and Clusters. Cambridge University Press (2010). Pp. 45–80.
[33] H.P. Bonze. Critical Rev. Solid State. Mater. Sci. **6**, *2*, 171 (1976).

Translated by A.Akhtyamov